



RESEARCH ARTICLE

A novel real-time tension distribution method for cable-driven parallel robots

Da Song¹, Ming Lu¹ , Lei Zhao¹ , Zhichao Sun¹, Haochen Wang¹ and Lixun Zhang²

¹School of Mechanical Engineering, Northeast Electric Power University, Jilin, China

²College of Mechanical and Electrical Engineering, Harbin Engineering University, Harbin, China

Corresponding author: Lei Zhao; Email: xa18944637307@gmail.com

Received: 17 May 2024; **Accepted:** 29 August 2024; **First published online:** 16 October 2024

Keywords: cable-driven parallel robots; force distribution; parallel robot; robot dynamics

Abstract

The tension distribution problem of cable-driven parallel robots is inevitable in real-time control. Currently, iterative algorithms or geometric algorithms are commonly used to solve this problem. Iterative algorithms are difficult to improve in real-time performance, and the tension obtained by geometric algorithms may not be continuous. In this paper, a novel tension distribution method for four-cable, 3-DOF cable-driven parallel robots is proposed based on the wave equation. The tension calculated by this method is continuous and differentiable, without the need for iterative computation or geometric centroid calculations, thus exhibiting good real-time performance. Furthermore, the feasibility and rationality of this algorithm are theoretically proven. Finally, the real-time performance and continuity of cable tension are analyzed through a specific numerical example.

1. Introduction

Cable-driven parallel robots (referred to as CDPRs or CDPR hereafter) are special parallel robots that use cables instead of rigid links to transmit motion and forces [1]. The flexible nature of cable-driven robots provides advantages over traditional parallel robots, such as low moving inertia, large workspace, high velocity, and low maintenance costs [2]. As a result, they have attracted considerable attention from researchers and have been widely applied in astronaut training [3], rehabilitation robotics [4], giant radio telescopes [5], and human-machine interaction devices [6].

The most basic model of CDPRs is the geometric model, which focuses on the robot's geometric layout and kinematics while simplifying the dynamics. This model traditionally assumes that the cables are idealized as precise linear distances between two points in space, specifically between the proximal anchor points on the fixed frame and the distal anchor points on the moving platform, with the distances perfectly matched. A common extension to the standard model (integrating geometry, dynamics, and control) is the inclusion of pulleys and friction [7–9]. For example, Mamidi et al. incorporated pulley kinematics based on the recursive sub-system-level Lagrangian multiplier approach (RSSLM) [10]. Fabritius et al. proposed a framework aiming to unify various CDPR models found in the literature. It consists of four nested CDPR model stages (point platform, geometric, elastic, and catenary) and two optional model extensions (force offset and pulleys) [11]. Patel et al. described a CDPR end effector considering pulleys by using closed-loop equations for cable lengths and cable length squares, as well as an unconstrained parameterization of the pose [12].

Due to the non-negligible mass and elasticity of the cables, the cables deform when the end effector moves [1, 13]. Therefore, in motion planning, it is more inclined to study the tension distribution of cables rather than their lengths. Since cables can only exert tension, redundancy is required to fully constrain the system [14, 15]. In other words, the number of cables m in CDPRs is greater than the number of degrees of freedom n of the end effector. This configuration is referred to as overconstrained,

and the redundancy is denoted as $r = m - n$. Typically, the redundancy is set to 1–3 [16]. However, for overconstrained systems, since m is not equal to n , the number of equations for cable tensions is smaller than the number of variables, resulting in infinitely many solutions for cable tensions [17]. At time t , the set of all solutions forms an r -dimensional linear subspace. The problem of force distribution in redundantly constrained CDPRs is inevitable and often time-consuming in control. Chawla et al. trained a neural network for the inverse statics (IKS) problem of CDPRs, providing solutions for both inverse statics and forward statics and significantly improving computational speed [18]. Martin-Parra et al. proposed a new design scheme, established the kinematic and static models of a new robot, verified the static model of the robot through an optimized interior point algorithm, and obtained cable force distributions for different end effector trajectories [19].

In order to obtain stable and continuous tension solutions (cable tension exhibits smooth temporal variation without abrupt changes) to address the redundancy problem in CDPRs, many scholars have constructed an objective function that treats the dynamics or statics equations of CDPRs as constraints, thereby transforming the problem of tension distribution of flexible cables into an optimization problem. Oh et al. utilized the 1-norm of the tension set as the objective function and provided methods for solving linear programming and quadratic programming problems to obtain feasible solutions within the operational space of the system [20]. Borgstrom proposed a new linear programming formulation that generates the optimal and safe tension distribution in CDPRs by introducing relaxation variables [21]. However, the solution obtained through 1-norm optimization is not continuous and may cause high-frequency vibrations [22]. Taghirad et al. introduced the 2-norm of the tension set as the objective function for solving the problem [23], while Gosselin et al. introduced the p -norm as the optimization objective [24]. Geng proposed an optimization algorithm based on the minimum tension-to-hyperstaticity ratio to address excessive stiffness [25]. However, most of these optimization algorithms are iterative, resulting in tension sets that often approach the lower limit of cable tension and lack real-time performance. Pott et al. proposed an iterative algorithm solely based on matrix operations [26, 27]. Fabritius et al. proposed a force correction method based on the null space to improve the dynamic performance of CDPRs. This method modifies the cable forces within the null space of the robot's structural matrix, keeping them within feasible limits and as close as possible to the desired level without altering the platform's posture [28]. Jin et al. introduced a modified index to evaluate the motion/force transmission performance of CDPRs in order to address the tension constraint of flexible cables. By calculating the power coefficients of positive and negative output motion directions, they ensured that the driving forces in the opposite directions of the two motion screws are positive. Furthermore, through optimization design based on the transmission index, CDPRs can reduce singularities in the workspace [29]. Einar Ueland et al. applied the logarithmic barrier method to construct the objective function and demonstrated its continuous differentiability with respect to the cable tensions at different time instances when it obtains the optimal solution [30]. They also introduced relaxation variables to enable rapid convergence of the proposed optimization problem, resulting in better real-time performance compared to other objective functions.

Due to the iterative nature of tension distribution algorithms based on optimization problems, geometric methods have attracted considerable attention from scholars. Marc Gouttefarde et al. introduced an algorithm for the tension feasible region (TFR) of n -DOF (degrees of freedom) CDPRs specifically designed for $n + 2$ cables driving n platforms. The algorithm determines the vertices of the 2-D convex polygon in either clockwise or counterclockwise direction and involves corresponding improvements to determine various cable tension distributions [31]. Cui et al. proposed a non-iterative optimization method for cable tension using the Graham scan method incorporated into the geometric approach. It was applied in a dual-thread PID force/position hybrid controller, providing a non-iterative method for optimizing the cable tension of CDPRs with $r = 2$, simultaneously addressing computational efficiency, minimizing cable tension, optimizing safety, and stiffness concerns [32]. Rodriguez-Barroso et al. presented a centroid-based approach to compute the polyhedron of cable tension possibilities, thereby calculating the maximum torque that can be exerted by a suspended cable-driven robot and determining the optimal tension distribution required to achieve any desired maximum torque [33].

Sun et al. developed a geometric tension feasible region algorithm by interpreting the TFR as the convex intersection of multiple boundary-parallel spaces, computing the tension feasible region for CDPRs with redundancy $r = 2$ and 3 [17]. Mohammad Reza Mousavi et al. proposed an algorithm applicable to redundancy levels $r = 1 - 3$, aiming to keep the cables within their tensile limits, preventing tearing during operations, defining limits on cable forces using a problem formulation, calculating the optimal solution for cable tension, tracking paths, and ensuring the safety of all actuators [34]. Geometric methods have several advantages, such as short computation time, applicability within the entire feasible workspace of force screws, and wide usage. They are the most widely used and popular non-iterative methods. With a good initial value, the computational cost of geometric methods can be significantly reduced. However, logical judgments are employed in each iteration step of geometric methods. Therefore, geometric methods cannot provide an explicit function for the optimal set of tensions [25]. Meanwhile, Einar Ueland et al. mentioned that the geometric algorithm involves the calculation of the 2-norm and pseudoinverse when calculating cable tension, which may result in discontinuous tension values [30].

This paper proposes a new force distribution algorithm for a CDPR with four cables and 3-DOF. Although many optimized iterative algorithms have been proposed to solve the redundancy constraint force distribution problem for CDPRs, issues with poor real-time performance have not been fully resolved, and there are certain requirements for hardware conditions. Additionally, geometric methods, when the redundancy r is 1, only use the geometric boundary of line segments for tension distribution. Due to insufficient research, effective tension analysis methods have not yet been provided for CDPRs with a redundancy of $r = 1$. This study begins with the wave equation from elastic dynamics to derive the coefficients that influence force distribution, enabling the distribution of cable forces without iterations and without the need for a complete calculation of the Jacobian matrix. Moreover, this paper investigates the impact of primary coefficients on cable tension, ensuring the continuity of tension. Lastly, a specific numerical example is presented to simulate and analyze the algorithm's real-time performance, the continuity, and the accuracy of the cable tension.

The organization of the paper is as follows: Section 2 introduces the wave equation. Section 3 starts from the general solution of the wave equation and derives an integral equation about the tension distribution coefficient of the cable, and proves the existence of a solution in the form of a cubic polynomial. Section 4 gives a specific numerical example to verify the correctness of the proposed algorithm, demonstrates its real-time performance, and compares it with existing methods. Section 5 summarizes the main features of this algorithm.

2. Introduction to the wave equation

The wave equation is a hyperbolic partial differential equation that describes wave propagation in continuum mechanics and physics. For an n -dimensional continuous medium, under zero initial conditions, the wave equation can be expressed as follows:

$$\begin{aligned}\square^2\phi &= -g(x) \\ \phi(\mathbf{x}, 0) &= \dot{\phi}(\mathbf{x}, 0) = 0\end{aligned}\quad (1)$$

Wherein, $\mathbf{x} = [x_1, x_2, \dots, x_n]$ represents the various axes/dimensions of the object of study. Its general solution is given by:

$$\phi(\mathbf{x}, t) = \frac{c_d}{2\pi\rho} \int_c \frac{g(\mathbf{x}', t')}{[c_d^2(t-t')^2 - h^2]^{\frac{1}{2}}} d\mathbf{x}' dt' \quad (2)$$

where $\square^2 = \nabla^2 - \frac{1}{c_d} \frac{\partial^2}{\partial t^2}$ is the wave operator, $\nabla^2 = \sum \frac{\partial^2}{\partial x_i^2}$ is the Laplacian operator, c_d is the propagation speed of the sound wave in the material of the end actuator, ρ is the density of the material of the end actuator, and $g(\mathbf{x})$ represents the external disturbance, which is the body force potential exerted on the

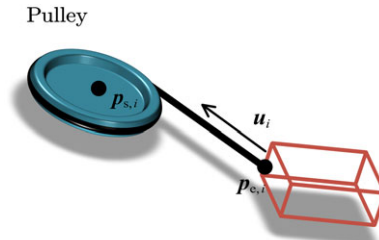


Figure 1. Schematic diagram of the *i*th pulley-cable-end actuator structure.

end actuator at point \mathbf{x} . ϕ represents the strain potential caused by the body force potential g , and the form of this general solution depends on the form of the external disturbance g .

3. Determination of tension distribution coefficients in flexible cable

The algorithm presented in this paper targets 3-DOF CDPs utilizing four cables, for which an elastic dynamic mathematical model of the end effector is established below. For a planar three-degree-of-freedom CDP, it usually has the structure shown in Figure 1.

Assuming that one of the forces acting on the end actuator is $\mathbf{F} = f(t)\delta(\mathbf{x} - \mathbf{p})\mathbf{i}_1$, where $\delta(\mathbf{x})$ is a two-dimensional Dirac function. According to vector field decomposition, \mathbf{F} can be decomposed as follows:

$$g = \nabla \cdot \mathbf{W}, \quad \mathbf{G} = -\nabla \times \mathbf{W} \tag{3}$$

$$f = \nabla g + \nabla \times \mathbf{G} = \nabla^2 \mathbf{W} \tag{4}$$

where g represents the volumetric expansion part in the displacement potential and \mathbf{G} represents the rotational part in the displacement potential, which is not considered in this paper. Eq. (4) is the Poisson equation. According to the theory of partial differential equations, its fundamental solution can be expressed in the following form:

$$\mathbf{W}(t) = \int_{V_x} \Phi(\mathbf{x} - \mathbf{x}') f dV \tag{5}$$

where:

$$\Phi(\mathbf{x}) = \begin{cases} -\frac{1}{2\pi} \ln |\mathbf{x}| & , n = 2 \\ \frac{\sqrt{\pi^n}}{\alpha(n)\Gamma(\frac{n}{2} + 1)} \frac{1}{|\mathbf{x}|} & , n > 2 \end{cases} \tag{6}$$

For $n = 2$, we have the following:

$$\mathbf{W}(\mathbf{x}, t) = -\frac{f(t)}{2\pi} \ln |\mathbf{x} - \mathbf{p}| \mathbf{i}_1 \tag{7}$$

$$g(\mathbf{x}, t) = \nabla \cdot \mathbf{W} = -\frac{f(t)}{2\pi} \frac{1}{r} \frac{\partial r}{\partial x_1} \tag{8}$$

$$[g(\mathbf{x}', t)] = -\frac{f(t - \frac{r}{c_d})}{2\pi \rho c_d^2} \frac{\partial}{\partial x_1} (\ln R) \tag{9}$$

where $r = \sqrt{(x_1 - p_1)^2 + (x_2 - p_2)^2}$, $R = \sqrt{(x'_1 - p_1)^2 + (x'_2 - p_2)^2}$, \mathbf{i}_1 represents the unit tensor or unit vector of \mathbf{x}_1 , $[\]$ represents the translation operator, and $[g(\mathbf{x}', t)]$ denotes the translation of the function

$g(\mathbf{x}', t)$ along the direction of \mathbf{x}_i . Substituting Eq. (2) yields:

$$\begin{aligned} \Phi(\mathbf{x}, t; \mathbf{p}_i) &= \frac{c_d}{2\pi} \int_{V_d} \frac{[g]}{[c_d^2(t-t')^2 - \rho^2]^{\frac{1}{2}}} dV_{x'} \\ &= \frac{1}{4\pi^2 c_d \rho} \int \frac{f(t-t' - \frac{h}{c_d})}{\sqrt{c_d^2(t-t')^2 - R^2}} \frac{\partial}{\partial x'_1} (\ln R) dx'_1 dx'_2 dt' \end{aligned} \tag{10}$$

On the circle determined by t' and h , $\frac{f(t-t' - \frac{h}{c_d})}{\sqrt{c_d^2(t-t')^2 - R^2}}$ is a constant value. Therefore, Eq. (10) can be rewritten as follows:

$$\Phi(\mathbf{x}, t; \mathbf{p}_i) = \frac{1}{4\pi^2 c_d \rho} \int \frac{f(t-t')}{\sqrt{c_d^2(t-t')^2 - h^2}} dh \cdot \int \frac{\partial}{\partial x'_1} (\ln R) dS \tag{11}$$

That is, first integrate along the circle determined by h and t' , and then integrate over h and t' .

Here, $h = c_d(t - t')$ is a variable dependent only on time, $\frac{\partial}{\partial x'_1} (\ln R)$ is an odd function with respect to x'_1 , and the integration domain S is a closed circular contour symmetric about x_1 . Therefore, when \mathbf{p}_i is inside S , the second half of the integral is 0; otherwise, it is $2\pi R^2$. Since the upper limit of the integration variable h can be replaced by r , and $h = c_d(t - t')$, Eq. (11) can be transformed to the following form:

$$\Phi(\mathbf{x}, t; \mathbf{p}_i) = \frac{1}{2\pi c_d \rho} \frac{\partial}{\partial x_1} \ln r \int \frac{f(t-t' - \frac{h}{c_d})}{\sqrt{c_d^2(t-t')^2 - h^2}} dt' dh \tag{12}$$

Now let's define the influence factor φ_i :

$$\varphi_i(t) = \int_S \Phi dx_1 dx_2 \tag{13}$$

Here, S represents the equivalent two-dimensional shape of the end effector. This influence factor represents the effect of applying force f at position \mathbf{p}_i on the end effector.

Let's define the influence coefficient λ_i :

$$\lambda_i = \varphi_i \left(\sum_i \varphi_i \right)^{-1} \tag{14}$$

Now, from the perspective of rigid body mechanics, let's establish the dynamic equation of the end effector:

$$\sum T_i = m \sum \ddot{\mathbf{x}}_i = m \ddot{\mathbf{p}}_d \tag{15}$$

Here, T_i represents the tension of the i th cable.

For CDPRSs, a commonly used approach to drive the end effector is by employing redundant cables, which exceed the degrees of freedom of the end effector. However, according to the theory of analytical mechanics, a planar rigid body can have at most three independent dynamic equations, while a planar CDPRS with three degrees of freedom requires a minimum of four cables. In other words, there is no one-to-one mapping between pushing from left to right and pushing from right to left as shown in Eq. (15). To address this issue, numerous scholars have proposed different solutions. These methods typically involve iterative and computationally complex calculations. Moreover, when applied to practical control, they are limited by hardware performance and struggle to meet real-time requirements. In this paper, an attempt is made to define the influence of each force on the end effector from the perspective of elastic dynamics in order to calculate all driving forces. Consequently, the following formulas are provided:

$$\begin{aligned} \sum_i T_i &= m \sum_i \ddot{\mathbf{p}}_i = m \ddot{\mathbf{p}}_d \\ \mathbf{p}_i &= \lambda_i \mathbf{p}_d \end{aligned} \tag{16}$$

Alternatively, it can be written as:

$$\mathbf{T}_i = \lambda_i m \mathbf{p}_d \tag{17}$$

Since ϕ is calculated based on the components of externally applied forces, Eq. (17) needs to be expressed in component form as follows:

$$T_{ij} = \lambda_{ij} m p_{dj} \tag{18}$$

Here, T_{ij} represents the j th component of the i th force T_i (distinct from the tensor). Considering that for CDPRs, the number of independent forces is equal to the number of independent cables, out of these eight components of T_{ij} , only four are independent. The relationship between these eight components will be established below.

It is not difficult to find that by substituting Eqs. (13) and (14) into Eq. (18), we obtain an integral equation about T_{ij} . To reduce the length, let $\xi = \sqrt{c_d^2(t - t')^2 - h^2}$ as follows:

$$T_{ij} = \frac{\int \left(\frac{\partial}{\partial x_1} \ln r \int \frac{[T_{ij}]}{\xi} dt' dh \right) d\Omega}{\sum_i \int \left(\frac{\partial}{\partial x_1} \ln r \int \frac{[T_{ij}]}{\xi} dt' dh \right) d\Omega} m \ddot{p}_{dj} \tag{19}$$

Since Eq. (19) is complex and difficult to solve, it is simplified as follows:

$$T_{i1} = \varphi_{i1} m \ddot{p}_{d1} \tag{20}$$

Making a variable substitution for φ_{ij} : $u = c_d(t - t')$, where $u \in (c_d t, 0)$, we obtain:

$$\varphi_{ij} = \int \frac{\partial}{\partial x_1} \ln r_i \int \frac{[T_{ij}]}{\sqrt{u^2 - h^2}} dh du d\Omega \tag{21}$$

Continuing the variable substitution by letting $h = u \sin \gamma$ and $dh = u \cos \gamma d\gamma$, where $\gamma \in (-\frac{\pi}{2}, \frac{\pi}{2})$, we have:

$$\varphi_{ij} = \int \frac{\partial}{\partial x_1} \ln r_i \int [T_{ij}] d\gamma du d\Omega \tag{22}$$

At this point, $[T_{ij}] = T_{ij} \left(\frac{u - u \sin \gamma}{c_d} \right)$. It can be verified that $\int [T_{ij}] d\gamma du$ is a function only dependent on time t , denoted as $G(t)$. Therefore, we obtain:

$$\varphi_{ij} = kG(t) \tag{23}$$

Clearly, $k = \int \frac{\partial}{\partial x_1} \ln r_i d\Omega$ is a physical parameter related to the shape of the end effector, which is constant for a given end effector. Substituting Eq. (23) back into Eq. (22), we have:

$$kG_{ij}(t) = k \int_{c_d t}^0 du \int_{-\frac{\pi}{2}}^{\frac{\pi}{2}} k[G_{ij}] m [\ddot{p}_{dj}] d\gamma \tag{24}$$

Taking the derivative of Eq. (24) with respect to t on both sides, we obtain:

$$\dot{G}_{ij}(t) = -C_p \int_{-\frac{\pi}{2}}^{\frac{\pi}{2}} [G_{ij}] [\ddot{p}_{dj}] d\gamma \tag{25}$$

In this case, $C_p = m k c_d$, and $[G_{ij}] = G(t(1 - \sin \gamma))$. Continuing with the variable substitution in Eq. (25), let $v = t(1 - \sin \gamma)$. Then $\gamma = \arcsin(1 - \frac{v}{t})$, and $d\gamma = \frac{1}{\sqrt{1 - (1 - \frac{v}{t})^2}} dv$ yields:

$$\dot{G}_{ij}(t) = -C_p \int_{2t}^0 \frac{G_{ij}(v) \ddot{p}_{dj}(v)}{\sqrt{1 - (1 - \frac{v}{t})^2}} dv \tag{26}$$

Eq. (26) is complex and difficult to solve. However, for engineering problems, it is often sufficient to find a particular solution that satisfies the engineering conditions. Due to the appealing properties of polynomials, this paper attempts to find a set of solutions that satisfy the aforementioned equation from the polynomial space. This paper provides the following set of solutions: when $G_{ij}(t)$ can be decomposed into the product of two rational polynomials, $g_1(t)$ and $g_2(t)$, where $g_2(t)$ is a quadratic polynomial, and let $\ddot{p}_{dj} = g_2(t)^{-1}$, then there must exist $G_{ij}(t)$ and $p_{dj}(t)$ that satisfy Eq. (26).

Proof: By performing a variable substitution in Eq. (26), let $\sin w = 1 - \frac{v}{t}$, then $dv = -t \cos w dw$, and $v = t(1 - \sin w)$.

$$\begin{aligned} \dot{G}_{ij}(t) &= C_p t \int_{-\frac{\pi}{2}}^{\frac{\pi}{2}} G_{ij}(t - t \sin w) \ddot{p}_{d1}(t - \sin w) dw \\ \frac{d}{dt}(g_1(t)g_2(t)) &= C_p t \int_{-\frac{\pi}{2}}^{\frac{\pi}{2}} g_1(t - t \sin w) dw \end{aligned} \tag{27}$$

Here, $g_1(t - t \sin w)$ is a polynomial in terms of $t - t \sin w$, and assume the i th term of g_1 is $a_i(t - t \sin w)^i = a_i t^i C_i^m (-\sin w)^{i-m}$. Therefore:

$$\begin{aligned} a_i t^i \int_{-\frac{\pi}{2}}^{\frac{\pi}{2}} C_i^m (-\sin w)^{i-m} dw &= \\ \begin{cases} 0, & \text{when } i \text{ and } m \text{ have different parity} \\ \frac{i-m-1}{i-m} \dots \frac{1}{2} \cdot \pi C_i^m a_i t^i, & \text{otherwise} \end{cases} \end{aligned} \tag{28}$$

It can be seen that after integrating the right side of Eq. (27), it remains a polynomial in terms of t , with a degree one higher than the original $g_1(t)$. Therefore, there should exist a polynomial G_{ij} of degree two higher than g_1 that satisfies Eq. (27). In other words, let g_2 be a quadratic polynomial in t , and Eq. (27) can be satisfied. Since the proof for higher-degree polynomials is not the focus of this paper, we only prove the existence of g_1 in quadratic polynomial form.

Let $g_1 = b_2 t^2 + b_1 t + b_0$ and $g_2 = (\ddot{p}_{d1}(t))^{-1} = c_1 t^2 + c_2 t + c_3$. Based on the equality of corresponding coefficients, the following system of equations can be obtained:

$$\mathbf{A} \mathbf{b} = 0 \tag{29}$$

where

$$\begin{aligned} \mathbf{A} &= \begin{bmatrix} 0 & 4c_3 & 4c_2 - C_p \\ 3c_3 - C_p & 3c_2 & 3c_1 \\ c_2 & c_1 & c_0 \\ c_1 & c_0 & 0 \end{bmatrix} \\ \mathbf{b} &= [b_0 \quad b_1 \quad b_2] \end{aligned} \tag{30}$$

It can be seen that in order for the above equations to have a solution, the rank of the matrix must be less than 3. When the relationships between the elements of $\mathbf{c} = [c_0 \ c_1 \ c_2]$ satisfy the conditions in the appendix, the rank of matrix \mathbf{A} is 2. That is, when the values of b_1, b_2, b_3, c_1, c_2 , and c_3 satisfy the conditions in the appendix, the assumption holds and the proof is complete.

Through the above proof, it can be found that the $G_{ij}(t)$ determined by p_{d1} is not unique. This is because the matrix \mathbf{A} does not have full rank, and any linear combination of its null vectors satisfies the equation set (29). From Eq. (27), it can be easily seen that any multiple β of the null vector can be absorbed into C_p . Therefore, the exact value of C_p is not important in the derivation process of the preceding formulas, as there always exists a suitable β to make C_p take any value.

3.1. Approximate calculation method for cable tension direction

After determining the tension components in either the horizontal or vertical orientation of the cable, the corresponding tension vector should be derived from the cable’s direction vector. An essential element in this process is the Jacobian matrix. Owing to the complexity of its rigorous calculation, this paper presents a simplified method for computing the Jacobian matrix.

As shown in Figure 2, under normal circumstances, the actual contact point slides within the dashed region of the $\frac{1}{4}$ arc. Calculating the Jacobian matrix directly using the real position of the contact point \mathbf{p}_r can be cumbersome. However, if we allow for some error, we can simplify the calculation of the cable tension direction and the subsequent Jacobian matrix by artificially fixing the contact point at

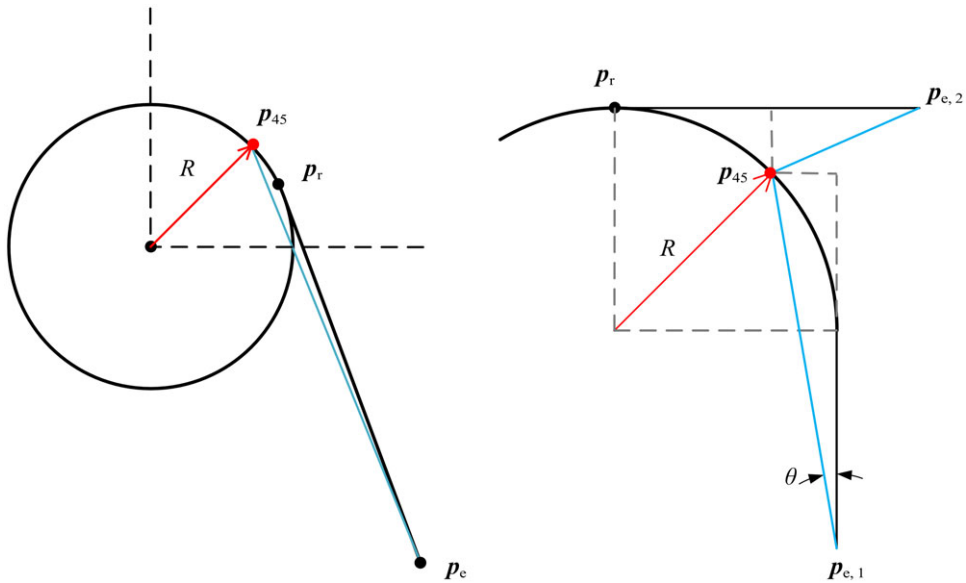


Figure 2. Illustration of tangent point and approximation point.

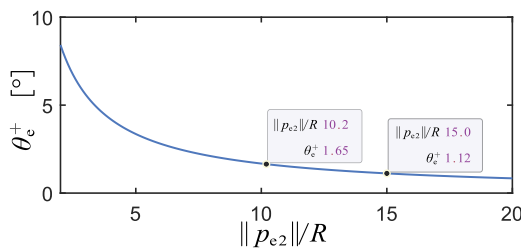


Figure 3. Variation of θ_e^+ with $R/\|p_{e,2}\|$.

position p_{45} on the arc, which forms a 45° angle with the x -axis. Since the cable direction vectors in the Jacobian matrix are normalized, this paper evaluates the algorithm’s error using angles. Let p_r be the actual contact point position, p_{45} be the artificially defined contact point position, and p_e be the end effector position. Based on geometric relationships, the maximum error in θ occurs at the position shown in the right figure of Figure 2. Assuming counterclockwise deviation is positive and clockwise deviation is negative, it can be inferred that the deviation lies within the range shown in Eq. (31).

$$\theta_e^- = 0$$

$$\theta_e^+ = \arcsin \left(\frac{R \left(1 - \frac{\sqrt{2}}{2} \right)}{\|p_{e,2} - p_{45}\|} \right) \tag{31}$$

According to Eq. (31), the maximum deviation value is independent of the pulley’s position. If we place the pulley at $(-R, -R)$, then p_{45} will be at the origin. In this case, $\theta_e^+ = R(1 - \frac{\sqrt{2}}{2})/\|p_{e,2}\|$, resulting in Figure 3. When the ratio is 10.2, the error is 1.6 degrees, and when the ratio is 15, the error is 1.1 degrees.

Let $u_i = u_{ij}$ ($i = x, y; j = 1, 2$) be the direction vectors of the cable tension. We have:

$$u_i = \frac{p_e - p_{45}}{\|p_e - p_{45}\|} \tag{32}$$

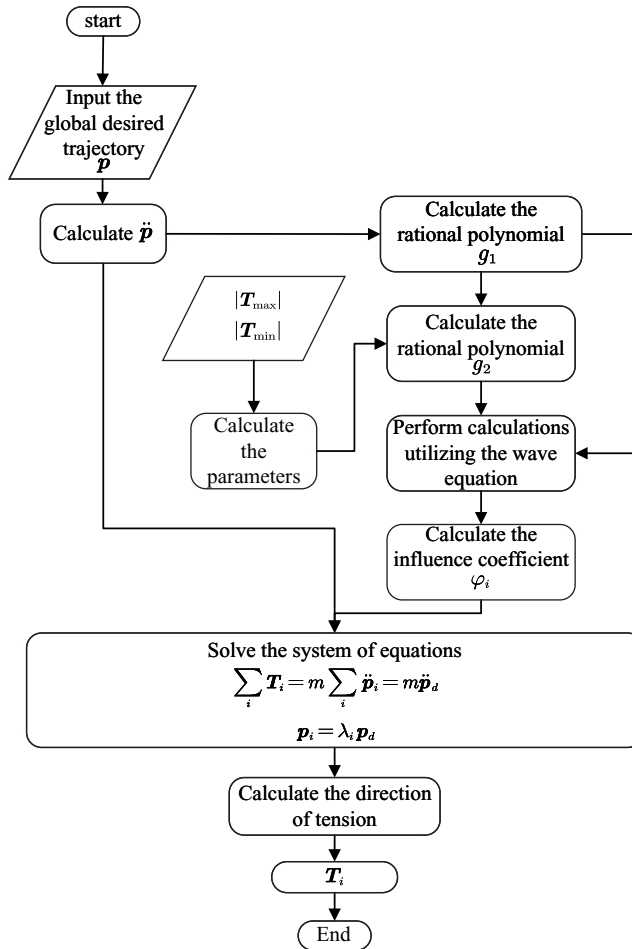


Figure 4. Flowchart of the tension distribution algorithm.

Therefore, the relationship between the magnitude and direction of the cable tension can be written as follows:

$$T_{ij} = \|T\|_i u_{ij} \quad (i = x, y; j = 1, 2) \quad (33)$$

3.2. The algorithm process

The specific process of the cable tension distribution algorithm introduced in this paper is depicted in Figure 4. It necessitates an understanding of the global desired trajectory and its second derivative to compute the coefficients for the time-varying tension distribution of the cables. This calculation can be considered pre-processing of the input signal, not part of the control strategy loop.

Unlike the cable tension distribution algorithms referenced in the introduction, which fully calculate the Jacobian matrix within the control strategy loop, this algorithm's optimization branch employs an iterative solution based on optimization theory, while the convex geometry branch uses the geometric attributes of shapes such as vertices, edges, and centroids for its calculations. These processes occur within the control strategy loop, endowing the proposed algorithm with a natural real-time performance advantage.

Table I. Values of the main parameters

Variable	Value	Variable	Value
C_p	4	b_0	-0.64
c_0	4.74	b_1	0.66
c_1	4.88	b_2	-0.41
c_2	2	β_1	-1.3
c_3	0.27	β_2	0.53

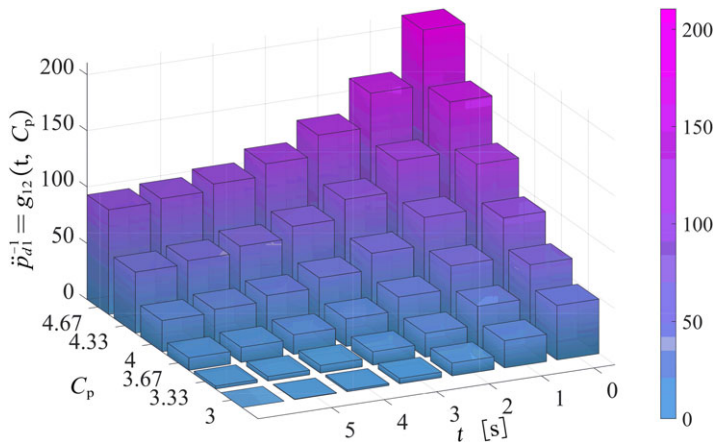


Figure 5. Influence of C_p on the trajectory.

4. Numerical Example

In this section, the aforementioned formulas are used to calculate a practical problem, and the influence of β on cable tension is discussed. The values of the main parameters in this paper are shown in Table I.

4.1. Influence of c_2 and C_p on end trajectory

By setting the rank of matrix \mathbf{A} to 2, it can be determined that the parameters of \mathbf{c} can be expressed as functions of c_2 and C_p . Therefore, their values directly affect the value of the end trajectory. Finally, it is determined that $c_2 = 2$ and $C_p = 4$.

4.2. Influence of β values on cable tension

Based on the values of the coefficients mentioned above, the specific values of each quantity can be calculated as follows (Figs. 5 and 6):

$$\mathbf{A} = \begin{bmatrix} 0.000 & 0.533 & 12.858 \\ -1.600 & 12.000 & -82.654 \\ 4.000 & -27.551 & 265.670 \\ -27.551 & 265.670 & 0 \end{bmatrix} \tag{34}$$

$$\mathbf{b} = \text{null}(\mathbf{A}) = [0.995 \quad 0.103 \quad -0.004] \tag{35}$$

So that:

$$\begin{aligned} g_{12}(t) &= g_{22}(t) \\ &= \ddot{p}_{d1}^{-1} = 0.27 t^3 + 2.00 t^2 + 4.88 t + 4.74 \end{aligned} \tag{36}$$

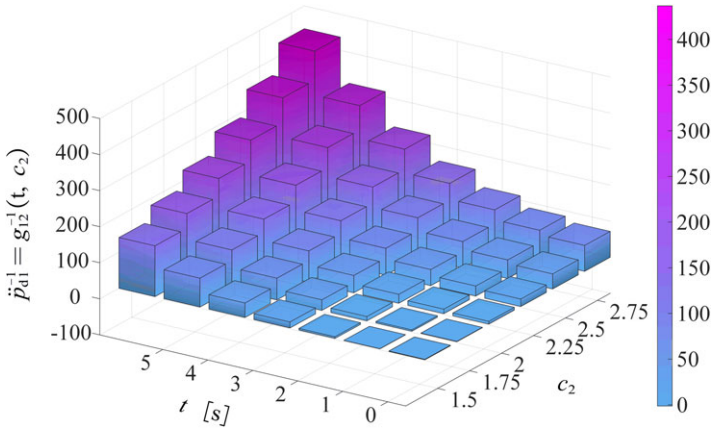


Figure 6. Influence of c_2 on the trajectory.

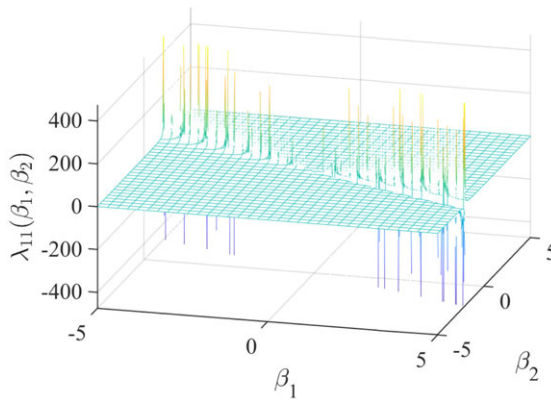


Figure 7. Influence of β on λ_{i1} .

$$\begin{aligned}
 g_{11}(t) &= \beta_1(-0.004 t^2 + 0.103 t + 0.995) \\
 g_{22}(t) &= \beta_2(-0.004 t^2 - 0.103 t + 0.995)
 \end{aligned}
 \tag{37}$$

Therefore, by substituting Eqs. (36), (37) into (20), (23), and (27), we can obtain the equation $\lambda_{i1} = \lambda_{i1}(\beta_1, \beta_2, t)$. This is a surface plot in four-dimensional space, making it difficult to obtain intuitive information. Hence, this paper uses $\lambda_{i1,max}$ to reflect the influence of β on λ_{ij} . Here, $\lambda_{i1,max}$ represents the extremum in the time direction. For the specific derivation process, please refer to the Appendix C. The three-dimensional surface plot can be referred to in Figure 7. It is easy to see that different rope tensions will directly affect the maximum value of the rope tension in the trajectory planning. Generally, the greater the rope tension, the stronger the anti-interference ability of the CDPR, so the rope tension should be as large as possible within the allowable output torque range of the motor. Considering all factors, the values of β_1 and β_2 can be chosen as shown in Table I.

4.3. Calculation of θ_d

When the cable tensions and end displacement are determined, the angle of the end effector is no longer arbitrary. This is because the angular displacement of the end effector of a CDPR (cable-driven parallel

robot) is coupled with its displacement, requiring the calculation of the end effector’s angular displacement based on the cable tensions and end trajectory. By applying the moment balance equation to the end effector, we have:

$$\begin{aligned}
 m \ddot{\theta}_d &= \sum_i f_i (\mathbf{r}_i \times \mathbf{u}_i) \\
 &= \sum_i f_i (r_{i1} u_{i2} - r_{i2} u_{i1})
 \end{aligned}
 \tag{38}$$

Here, \mathbf{r}_i and \mathbf{u}_i represent the position vector and unit vector of cable i , respectively. Thus, it can be known that:

$$\theta_d = \int_0^t \left(\int_0^t \ddot{\theta}_d dt \right) dt
 \tag{39}$$

For an arbitrarily complex trajectory, its θ_d generally cannot be analytically solved. The reason is that \mathbf{u}_i in Eq. (38) is a function of θ . Therefore, in the subsequent simulation, numerical integration will be used for Eq. (39) (Figure 8).

4.4. Simulation analysis

Based on the previous selection, the expression for p_{d1} can be reverse calculated as follows:

$$\begin{aligned}
 \mathbf{p}_{d1} &= (p_{d1}, p_{d2}, p_{d3}) \\
 p_{d1} &= 0.53 (t + 4.08) \log (t + 4.08) \\
 &\quad - 0.62 \log ((t + 1.71)^2 + 1.428) \\
 &\quad - 0.26 (t + 1.71) \log ((t + 1.71)^2 + 1.43) \\
 &\quad - 0.63 (t + 1.71) \operatorname{atan} (0.84 t + 1.43) \\
 &\quad + 1.04 \operatorname{atan} (0.84 t + 1.43) - 1.2 t - 3.5 \\
 p_{d2} &= p_{d3} = 0
 \end{aligned}
 \tag{40}$$

The values of λ_{i1} at this time are as follows:

$$\begin{aligned}
 \lambda_{11} = \lambda_{41} &= \frac{-2.16 t^2 - 3.47 t + 3.37}{3.14 t^2 - 12.00 t + 11.64} \\
 \lambda_{21} = \lambda_{31} &= \frac{4.77 t^2 - 7.68 t + 7.45}{2.82 t^2 - 10.80 t + 10.48}
 \end{aligned}
 \tag{41}$$

Substituting into Eq. (20), we can obtain the values of T_{11} and T_{41} :

$$\begin{aligned}
 T_{11} = T_{41} &= \frac{345.37 t^2 - 555.87 t + 539.30}{T_{\text{den}}} \\
 T_{21} = T_{31} &= \frac{847.13 t^2 - 1363.46 t + 1322.78}{T_{\text{den}}} \\
 T_{\text{den}} &= 8.47 t^5 + 30.33 t^4 - 55.46 t^3 \\
 &\quad - 203.99 t^2 - 6.72 t + 551.64
 \end{aligned}
 \tag{42}$$

Substituting Eq. (42) into Eq. (33), the tension $|T_i|$ of the cable can be obtained. Furthermore, dynamic simulations yield the results shown in Figure 9(a). Figure 9(b) displays the simulated trajectory and error obtained using the Newton Slack Any P method [30]. Here, p_{ci} represents the simulated trajectory in the i th direction, and p_{eri} represents the error between the simulated trajectory and the desired trajectory ($i = x, y$).

From Figure 8, it can be observed that the cable tension calculated using the proposed method is continuous. Figure 9 demonstrates that the results obtained from dynamic simulations using the proposed tension distribution method align well with the desired trajectory. Running the simulation trajectory 20

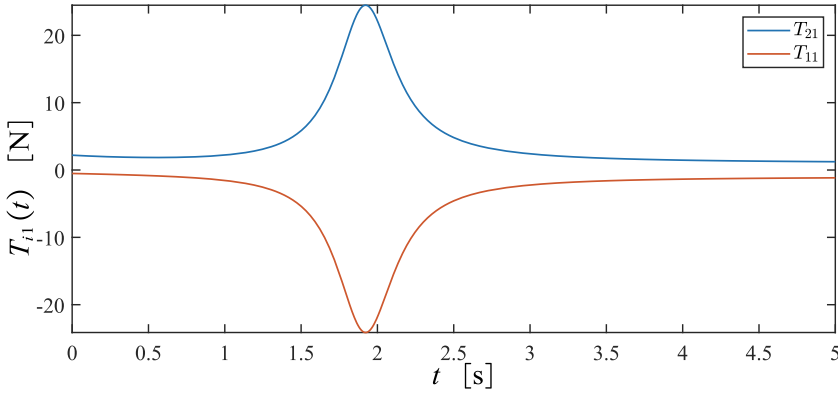


Figure 8. Tension of the cable in the x direction.

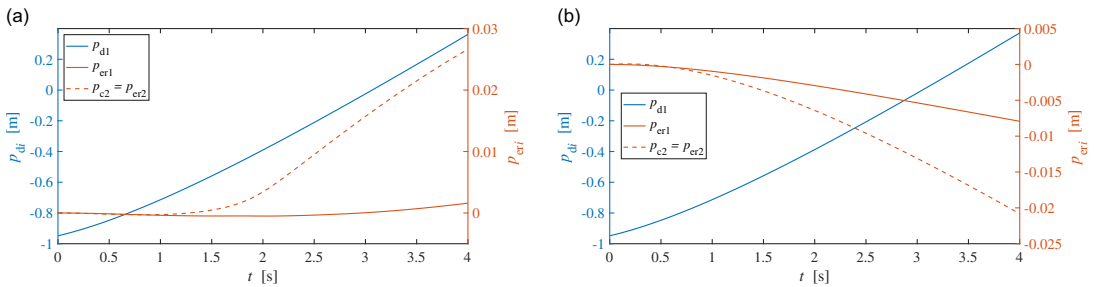


Figure 9. (a) Simulated trajectory and error in the *i*th direction using the proposed method. (b) Simulated trajectory and error in the *i*th direction using the Newton Slack Any P method (*i* = 1, 2).

times and taking the average runtime yields an average time of 31.44 s for the simulation model using the proposed cable tension distribution method, while the average runtime for the simulation program using the Newton Slack Any P method is 35.37 s.

5. Conclusion

From the wave equation, this paper defines the influence factor ϕ_i of the *i*th cable on the end effector and defines the influence coefficient λ_{ij} to allocate the cable tension. A mathematical model is established for λ_{ij} and \ddot{p}_{d1} , and it is proven that it has a solution in at least cubic polynomial form. This solution is a rational polynomial fraction form, which is computationally simple and can better meet real-time force allocation requirements. Finally, a specific numerical example is provided to verify the correctness of the algorithm and demonstrate its real-time capability. A simple comparison is made with the Newton Slack Any P method proposed by scholar Einar Ueland. However, when using this algorithm, if the position of the end effector is specified, its angle cannot be freely determined. Part of the reason is that the solution provided by this algorithm is not the solution in the entire space, but a curve in the solution space. Another reason is that the position and angle of CDPRs are strongly coupled, and specifying the displacement and angular displacement of the end effector does not necessarily result in a force helix curve within the feasible space of CDPRs.

Our team’s future work includes the following: (1) Planning to change λ_{ij} to expand the range of trajectories applicable to this algorithm, aiming to make this algorithm usable for any curve within the feasible space of force helices in CDPRs. (2) Planning to introduce a friction model to more comprehensively describe and predict the behavior of cables in actual operations. (3) Expanding the range of applications for the algorithm, not limited to four-cable 3-DOF CDPRs, extending to spatial CDPRs.

Author contributions. Da Song, Ming Lu, and Lei Zhao completed the main part of the theoretical derivation. Zhichao Sun and Haochen Wang participated in the theoretical simulation and translation of the paper. Lixun Zhang provides special guidance in the theoretical part of this paper.

Financial support. Supported by the National Natural Science Foundation of China (Grant No. 61773007) and the Jilin Provincial Natural Science Foundation of China (Grant No. YDZJ202301ZYTS272)

Competing interests. The authors declare no conflicts of interest exist.

Ethical approval. Not applicable.

References

- [1] T. K. Mamidi and S. Bandyopadhyay, “A modular computational framework for the dynamic analyses of cable-driven parallel robots with different types of actuation including the effects of inertia, elasticity and damping of cables,” *Robotica* **42**(5), 1676–1708 (2024).
- [2] S. Qian, Z. Zhao, P. Qian, Z. Wang and B. Zi, “Research on workspace visual-based continuous switching sliding mode control for cable-driven parallel robots,” *Robotica* **42**(1), 1–20 (2024).
- [3] L. Zhang, Y. Zou, L. Wang and X. Pei, “Hybrid force control based on ICMAC for an astronaut rehabilitative training robot regular paper,” *Int. J. Adv. Robot. Syst.* **9**(2), 55 (2012).
- [4] M. Khadem, F. Inel, G. Carbone and A. S. T. Tich, “A novel pyramidal cable-driven robot for exercising and rehabilitation of writing tasks,” *Robotica* **41**(11), 3463–3484 (2023).
- [5] B. Duan, Y. Qiu, F. Zhang and B. Zi, “On design and experiment of the feed cable-suspended structure for super antenna,” *Mechatronics* **19**(4), 503–509 (2009).
- [6] A. Fortin-Côté, P. Cardou and C. Gosselin, “An admittance control scheme for haptic interfaces based on cable-driven parallel mechanisms,” *2014 IEEE International Conference on Robotics and Automation (ICRA)* (2014) pp. 819–825.
- [7] W. Kraus, M. Kessler and A. Pott, “Pulley friction compensation for winch-integrated cable force measurement and verification on a cable-driven parallel robot,” *2015 IEEE International Conference on Robotics and Automation (ICRA)* (2015) pp. 1627–1632.
- [8] X. Hu, L. Cao, Y. Luo, A. Chen, E. Zhang and W. Zhang, “A novel methodology for comprehensive modeling of the kinetic behavior of steerable catheters,” *IEEE/ASME Trans. Mechatr.* **24**(4), 1785–1797 (2019).
- [9] Y. Liu, J. Li, Z. Zhang, X. Hu and W. Zhang, “Experimental comparison of five friction models on the same test-bed of the micro stick-slip motion system,” *Mech. Sci.* **6**(1), 15–28 (2015).
- [10] T. K. Mamidi and S. Bandyopadhyay, “A computational framework for the dynamic analyses of cable-driven parallel robots with feed and retrieval of cables,” *Mech. Mach. Theory* **186**, 105338 (2023).
- [11] M. Fabritius, P. Miermeister, W. Kraus and A. Pott, “A framework for analyzing the accuracy, complexity, and long-term performance of cable-driven parallel robot models,” *Mech. Mach. Theory* **185**, 105331 (2023).
- [12] S. Patel, V. L. Nguyen and R. J. Caverly, “Forward kinematics of a cable-driven parallel robot with pose estimation error covariance bounds,” *Mech. Mach. Theory* **183**, 105231 (2023).
- [13] M. Peng, L. Xiao, Q. Chen, G. Wei, Q. Lin and J. Zhuo, “Dynamic modeling and characterization of compliant cable-driven parallel robots containing flexible cables,” *Robotica* **41**(10), 3160–3174 (2023).
- [14] G. Abbasnejad, J. Eden and D. Lau, “Generalized ray-based lattice generation and graph representation of wrench-closure workspace for arbitrary cable-driven robots,” *IEEE Trans. Robot.* **35**(1), 147–161 (2018).
- [15] M. Ding, X. Zheng, L. Liu, J. Guo and Y. Guo, “Collision-free path planning for cable-driven continuum robot based on improved artificial potential field,” *Robotica* **42**(5), 1350–1367 (2024).
- [16] V. Ferravante, E. Riva, M. Taghavi, F. Braghin and T. Bock, “Dynamic analysis of high precision construction cable-driven parallel robots,” *Mech. Mach. Theory* **135**, 54–64 (2019).
- [17] G. Sun, Z. Liu, H. Gao, N. Li, L. Ding and Z. Deng, “Direct method for tension feasible region calculation in multi-redundant cable-driven parallel robots using computational geometry,” *Mech. Mach. Theory* **158**, 104225 (2021).
- [18] I. Chawla, P. Pathak, L. Notash, A. Samantaray, Q. Li and U. Sharma, “Inverse and forward kineto-static solution of a large-scale cable-driven parallel robot using neural networks,” *Mech. Mach. Theory* **179**, 105107 (2023).
- [19] A. Martín-Parra, S. Suarez-Perez, A. Gonzalez-Rodriguez, A. G. Gonzalez-Rodriguez, A. I. Lopez-Diaz and G. Rubio-Gomez, “A novel design for fully constrained planar cable-driven parallel robots to increase their wrench-feasible workspace,” *Mech. Mach. Theory* **180**, 105159 (2023).
- [20] S.-R. Oh and S. K. Agrawal, “Cable suspended planar robots with redundant cables: Controllers with positive tensions,” *IEEE Trans. Robot.* **21**(3), 457–465 (2005).
- [21] P. H. Borgstrom, B. L. Jordan, G. S. Sukhatme, M. A. Batalin and W. J. Kaiser, “Rapid computation of optimally safe tension distributions for parallel cable-driven robots,” *IEEE Trans. Robot.* **25**(6), 1271–1281 (2009).
- [22] T. Bruckmann, A. Pott and M. Hiller, “Calculating Force Distributions for Redundantly Actuated Tendon-Based Stewart Platforms,” *In: Advances in Robot Kinematics: Mechanisms and Motion* (Springer, 2006) pp. 403–412.

[23] H. D. Taghirad and Y. B. Bedoustani, "An analytic-iterative redundancy resolution scheme for cable-driven redundant parallel manipulators," *IEEE Trans. Robot.* **27**(6), 1137–1143 (2011).

[24] C. Gosselin and M. Grenier, "On the determination of the force distribution in overconstrained cable-driven parallel mechanisms," *Meccanica* **46**(1), 3–15 (2011).

[25] X. Geng, M. Li, Y. Liu, Y. Li, W. Zheng and Z. Li, "Analytical tension-distribution computation for cable-driven parallel robots using hypersphere mapping algorithm," *Mech. Mach. Theory.* **145**, 103692 (2020).

[26] A. Pott, "An improved force distribution algorithm for over-constrained cable-driven parallel robots," *Computational Kinematics: Proceedings of the 6th International Workshop on Computational Kinematics (CK2013)* (2014) pp. 139–146.

[27] A. Pott and T. Bruckmann, *Cable-Driven Parallel Robots* (Springer, 2013).

[28] M. Fabritius, G. Rubio-Gómez, C. Martin, J. C. Santos, W. Kraus and A. Pott, "A nullspace-based force correction method to improve the dynamic performance of cable-driven parallel robots," *Mech. Mach. Theory* **181**, 105177 (2023).

[29] X. Jin, W. Ye and Q. Li, "New indices for performance evaluation of cable-driven parallel robots: Motion/force transmissibility," *Mech. Mach. Theory* **188**, 105402 (2023).

[30] E. Ueland, T. Sauder and R. Skjetne, "Optimal force allocation for overconstrained cable-driven parallel robots: Continuously differentiable solutions with assessment of computational efficiency," *IEEE Trans. Robot.* **37**(2), 659–666 (2021).

[31] M. Gouttefarde, J. Lamaury, C. Reichert and T. Bruckmann, "A versatile tension distribution algorithm for n -dof parallel robots driven by $n + 2$ cables," *IEEE Trans. Robot.* **31**(6), 1444–1457 (2015).

[32] Z. Cui, X. Tang, S. Hou and H. Sun, "Non-iterative geometric method for cable-tension optimization of cable-driven parallel robots with 2 redundant cables," *Mechatronics* **59**, 49–60 (2019).

[33] A. Rodriguez-Barroso and R. Saltaren, "Tension planner for cable-driven suspended robots with unbounded upper cable tension and two degrees of redundancy," *Mech. Mach. Theory* **144**, 103675 (2020).

[34] M. R. Mousavi, M. Ghanbari, S. A. A. Moosavian and P. Zarafshan, "Rapid and safe wire tension distribution scheme for redundant cable-driven parallel manipulators," *Robotica* **40**(7), 2395–2408 (2022).

Appendix A. Condition for Rank-2 of A

There are multiple methods to determine the rank-2 condition of **A**, and this paper provides the following method:

$$\begin{aligned}
 a_{e1} &= -\frac{16 C_p^2}{75} \\
 a_{e2} &= -\frac{4 C_p \left(4 c_2 - \frac{\pi C_p}{2}\right)^2}{5} \\
 &\quad - \frac{8 C_p \left(4 c_2^2 - \frac{\pi C_p c_2}{2}\right)}{5} \\
 &\quad + \frac{8 C_p c_2 \left(4 c_2 - \frac{\pi C_p}{2}\right)}{5} \\
 a_{e3} &= 6 c_2 \left(4 c_2 - \frac{\pi C_p}{2}\right) \left(4 c_2^2 - \frac{\pi C_p c_2}{2}\right) \\
 &\quad - 3 \left(4 c_2^2 - \frac{\pi C_p c_2}{2}\right)^2 \\
 c_1 &= \frac{-a_{e2} + \sqrt{a_{e2}^2 - 4 a_{e1} a_{e3}}}{2 a_{e1}} \\
 c_0 &= \frac{4 c_1^2 c_2 - \frac{\pi}{2} c_1^2 C_p}{4 c_1 c_3 + 4 c_2^2 - \frac{\pi}{2} C_p} \tag{43}
 \end{aligned}$$

Where c_2 and C_p are arbitrary real numbers, and c_0 and c_1 determined by Eq. (43) make the rank of **A** equal to 2.

Appendix B. Integral form of \ddot{p}_{d1} in the real number domain

For the integration of \ddot{p}_{d1} , the most complex case arises when \ddot{p}_{d1}^{-1} has only one intersection with the x -axis (which is the case provided in this paper). In this situation, it has a pair of complex conjugate

roots, and the integration of \dot{p}_{d1} obtained by conventional methods is a complex solution. However, from a graphical perspective, the area enclosed by \ddot{p}_{d1} , $t = 0$, and the t -axis is a real number (a real function). From a mathematical point of view, the solution in the complex number domain (complex function solution) can always be simplified into a complex number (complex function) with a nonzero real part and a zero imaginary part. However, this is often difficult or even impossible to achieve. Therefore, in this paper, an integration method is proposed to avoid using complex numbers.

Assume that when $\ddot{p}_{d1}(t)$ has one real solution t_0 and a pair of complex conjugate solutions $t_r + t_i i$ and $t_r - t_i i$, the following equation holds:

$$\ddot{p}_{d1}(t) = \frac{1}{c_3(t - t_0)((t - t_r)^2 + t_i^2)} \tag{44}$$

Assume:

$$\ddot{p}_{d1}(t) = \frac{1}{c_3} \left(\frac{e_1}{t - t_0} + \frac{e_2 t + e_3}{(t - t_r)^2 + t_i^2} \right) \tag{45}$$

By equating the coefficients in Eqs. (44) and (45), the following system of Eq. (46) is obtained:

$$\mathbf{A}_p \mathbf{e} = [0 \quad 0 \quad 1]^T \tag{46}$$

Where:

$$\mathbf{A}_p = \begin{bmatrix} 1 & 1 & 0 \\ -2 t_r & -t_0 & 1 \\ t_i^2 + t_r^2 & 0 & -t_0 \end{bmatrix} \tag{47}$$

$$\mathbf{e} = [e_1 \quad e_2 \quad e_3]^T \tag{48}$$

Solving Eq. (46) yields:

$$\mathbf{e} = \mathbf{A}_p^{-1} \begin{bmatrix} 0 \\ 0 \\ 1 \end{bmatrix} = \begin{bmatrix} \frac{1}{t_r^2 + t_r^2 + 2 t_0 t_r - t_0} \\ -\frac{1}{t_i^2 + t_r^2 + 2 t_0 t_r - t_0} \\ \frac{2 t_r}{t_r^2 + t_r^2 + 2 t_0 t_r - t_0} \end{bmatrix} \tag{49}$$

At this point, the difficult-to-integrate part in Eq. (45) is reduced to the second half, given by:

$$\frac{e_2 t + e_3}{(t - t_r)^2 + t_i^2} = \frac{e_2}{2} \left(\frac{2 t - 2 t_r}{(t - t_r)^2 + t_i^2} + \frac{2 e_3 / e_2 + 2 t_r}{(t - t_r)^2 + t_i^2} \right) \tag{50}$$

At this point, it can be easily obtained that:

$$\begin{aligned} \dot{p}_{d1} &= \int_0^t \ddot{p}_{d1}(\tau) d\tau \\ &= \frac{1}{c_3} \int_0^t \frac{e_1}{\tau - t_0} d\tau + \frac{e_2}{2 c_3} \int_0^t \frac{2 \tau - 2 t_r}{(\tau - t_r)^2 + t_i^2} d\tau \\ &\quad + \frac{e_3 + e_2 t_r}{c_3} \int_0^t \frac{1}{(\tau - t_r)^2 + t_i^2} d\tau \end{aligned} \tag{51}$$

After rearranging, we obtain:

$$\begin{aligned} \dot{p}_{d1} &= \frac{e_1}{c_3} \ln(t - t_0) + \frac{e_2}{2 c_3} \ln((t - t_r)^2 + t_i^2) \\ &\quad + \frac{e_3 + e_2 t_r}{c_3 t_i} \operatorname{atan} \frac{t - t_r}{t_i} \end{aligned} \tag{52}$$

Continuing the integration, we have:

$$\begin{aligned}
 p_{d1} = & \frac{e_1}{c_3} (-t + (t - t_0) \ln (t - t_0)) \\
 & + \frac{e_2}{2 c_3} \left(-2 t + 2 t_i \operatorname{atan} \left(\frac{t - t_r}{t_i} \right) \right. \\
 & + \log \left((t - t_r)^2 + t_i^2 \right) (t - t_r) \\
 & + \frac{e_3 + e_2 t_r}{c_3 t_i} \left((t - t_r) \operatorname{atan} \frac{(t - t_r)}{t_i} \right. \\
 & \left. \left. - \frac{t_r}{2} \ln \left((t - t_r)^2 + t_i^2 \right) \right) \right) \quad (53)
 \end{aligned}$$

Combining Eqs. (49) and (53), we obtain the real function integral solution of the integrand with a third-degree polynomial in the denominator, which has complex conjugate roots in the numerator.

Appendix C. Calculation method for $\lambda_{i1, \max}$

Substituting g_{11} and g_{21} into Eqs. (23) and (14), we can obtain:

$$\lambda_{i1} = \lambda_{i1}(b_0, b_1, b_2, \beta_1, \beta_2, t) \quad (54)$$

Taking the partial derivative of the above equation with respect to t , we have:

$$\begin{aligned}
 \frac{\partial \lambda_i}{\partial t} = & \frac{(-2 b_1 b_2 \beta_1 \beta_2) t^2 + (-4 b_0 b_2 \beta_1 \beta_2) t}{d_4 t^4 + d_3 t^3 + d_2 t^2 + d_1 t + d_0} \\
 d_4 = & (b_2^2 \beta_1^2 + 2 b_2^2 \beta_1 \beta_2 + b_2^2 \beta_2^2) \\
 d_3 = & (2 b_1 b_2 \beta_1^2 - 2 b_1 b_2 \beta_2^2) \\
 d_2 = & (b_1^2 \beta_1^2 - 2 b_1^2 \beta_1 \beta_2 + b_1^2 \beta_2^2 \\
 & + 2 b_0 b_2 \beta_1^2 - 2 b_0 b_2 \beta_2^2) \\
 d_1 = & (2 b_0 b_1 \beta_1^2 - 4 b_0 b_1 \beta_1 \beta_2 + 2 b_0 b_1 \beta_2^2) \\
 d_0 = & b_0^2 \beta_1^2 - 2 b_0^2 \beta_1 \beta_2 + b_0^2 \beta_2^2 \quad (55)
 \end{aligned}$$

It is not difficult to observe that Eq. (55) has monotonic intervals with respect to t as $(0, -\frac{b_0}{b_1})$ and $(-\frac{b_0}{b_1}, +\infty)$. Therefore, substituting $t = -\frac{b_0}{b_1}$ along with b_0 , b_1 , and b_2 back into Eq. (54), we obtain the three-dimensional surface plot of $\lambda_{i1, \max} = \lambda_{i1}(\beta_1, \beta_2)$, showing the maximum value on t varying with β_1 and β_2 .